Food Hydrocolloids 103 (2020) 105616

Contents lists available at ScienceDirect

Food Hydrocolloids

journal homepage: http://www.elsevier.com/locate/foodhyd

Interfacial viscoelasticity and aging effect on droplet formation and breakup

Gerard Giménez-Ribes, Leonard M.C. Sagis, Mehdi Habibi *

Physics and Physical Chemistry of Foods, Wageningen University, Bornse Weilanden 9, 6708WG, Wageningen, the Netherlands

ARTICLE INFO

Keywords:
Viscoelastic interfaces
Drop formation
Capillary breakup
Surface rheology
Surfactant
SDS
Escin
β-Lactoglobulin
Bovine serum albumin

ABSTRACT

Interfacial rheology of interfaces stabilized by food ingredients has been studied extensively within the limits of small and slow deformations, within the linear viscoelastic regime (LVR). However, in practice, products such as foams or emulsions undergo fast and large deformations during food processes such as chewing. emulsifying, or foaming. In this study, we used capillary break-up and droplet formation to observe and quantify large and fast deformations of such interfaces, in the presence of surface viscoelasticity. We studied the inertial thinning of the liquid neck during drop formation using high-speed imaging. We tested solutions of several surface active molecules, including two low molecular weight surfactants (SDS and Tween 20), two milk proteins (β-Lactoglobulin, Bovine Serum Albumin) and the saponin Escin. Escin showed the most significant effect on the shape of the neck and neck thinning dynamics. Interfacial shear rheology measurements indicated that the unusual breakup observation of Escin solutions was related to the high viscoelastic surface shear moduli. These high moduli, and the resulting more symmetric and shorter neck shape observed for the proteins and Escin, are associated with the formation of solid-like interfacial structures. However, the presence of a viscoelastic interface did not affect the inertial thinning regime, which indicates that the solid structures were broken down locally at the area of minimum radius (R_{min}), and affected only the shape outside this region. The results of this work therefore, show that interfacial measurements within the LVR are not entirely representative for fast and large deformations well beyond linearity.

1. Introduction

Emulsions such as mayonnaise or salad dressing, and foams such as whipped cream or mousse are ubiquitous in the food industry (Sagis & Fischer, 2014). In these systems, the material properties are largely determined by properties of their fluid-fluid interfaces. Fast adsorption of surfactants at the interfaces is crucial for production of foams or emulsions, otherwise they tend to instantly show phase separation. However, the fast adsorption of the surfactant at the interface does not necessarily guarantee the stability of these systems over time. The stability of the foam or emulsion is determined by the properties of the adsorbed layer, such as structure, charge, thickness and interfacial rheology (McClements, 2007). In rapid processes such as emulsification, the dynamic surface tension is a better indication than the equilibrium one to determine how the interface behaves under deformations (Bos & Van Vliet, 2001). This is already known for low molecular weight surfactants (LMWS) that do not self-assemble into complex 2D interfacial microstructures. However, when the surface-active molecules tend to self-assemble into interfacial 2D structures such as gels or soft glasses, the interfacial dynamics will be governed not only by dynamic surface tension but also by the interfacial rheological properties of the interfaces (Sagis & Fischer, 2014).

Surface rheological properties such as the surface shear and dilatational modulus can be determined by applying sinusoidal deformations on the interface and measuring the material responses. When the deformation is small, the response would be in the linear regime, and Fourier transformation of the signal will generate only the first (fundamental) harmonic, of which the phase shift and intensity are used to calculate the storage and loss modulus. For large deformation, the responses enter the nonlinear regime, and higher harmonics will appear in the frequency spectrum (Sagis & Fischer, 2014). Different methods such as Lissajous curves, the representation of the stress in the form of Fourier series, or decomposition into Chebyshev orthogonal polynomials (Sagis & Fischer, 2014) can be used to quantify the nonlinear rheological response of an interface in large deformations. For all these methods, limitations arise due to the measuring equipment. These limitations

* Corresponding author.
E-mail address: mehdi.habibi@wur.nl (M. Habibi).

https://doi.org/10.1016/j.foodhyd.2019.105616
Received 6 August 2019; Received in revised form 18 December 2019; Accepted 20 December 2019
Available online 13 January 2020

become significant when rapid deformation of the interface need to be considered. For instance, when determining dilatational moduli with a profile analysis tensiometer (PAT), hydrodynamic effects at high-frequency oscillations will cause the drop shape to deviate from that predicted by the Young-Laplace equation, due to non-radial oscillations (Ravera, Loglio, & Kovalchuk, 2010). High-frequency oscillatory surface shear rheology is another example where inertial effects in the sub-phase fluid cause errors that should be corrected (Reynaert, Brooks, Moldenaers, Vermant, & Fuller, 2008; Vandebril, Franck, Fuller, Moldenaers, & Vermant, 2010).

Droplet and bubble formation at a nozzle often occur at very small time scales with considerable deformation of the interfaces. Therefore, this offers a suitable system to look into fast and large deformations of the interface. When the droplet approaches pinch-off, a fluid neck forms between the nozzle and the droplet (Fig. 1). Similar behavior occurs for bubble pinch-off (Pahlavan, Stone, McKinley, & Juanes, 2019). For a drop hanging from a nozzle, the total volume which can be supported before detaching is dependent on the surface tension and weight. The relative importance of these two forces is represented by the Eötvös or Bond number, $Eo = \frac{\Delta\rho g R^2}{\gamma}$, where γ is the surface tension, $\Delta\rho$ is the density difference between the droplet liquid and its surrounding, g is the gravitational acceleration and R is the droplet radius (Yarin, 2006) . The balance between inertial and viscous stresses, and between inertial and interfacial stresses are given, respectively, by the Reynolds number ($Re = \frac{\rho v d}{\eta}$) and the Weber number ($We = \frac{\rho v^2 d}{\gamma}$)(Christanti & Walker, 2001), where ρ is the density, υ is the jet velocity, d is the diameter of the liquid jet, and η is the viscosity. From these numbers the Ohnesorge number (Oh) can be obtained, which is a dimensionless parameter used to classify different regimes at breakup: $Oh = \frac{We^{1/2}}{Re} = \frac{\eta}{(\rho\gamma d)^{1/2}}$. The Ohnesorge number compares the time scales of viscosity with the inertial time scale (Mathues, McIlroy, Harlen, & Clasen, 2015). When the viscosity of the liquid is high, it will overcome the effect of capillary forces, and therefore $Oh^{-1} = 0$, which is identified as the Viscous regime (V) (Papageorgiou, 1995). When Oh is neither close to 0 nor tends to infinity, then the thinning of the neck radius follows the Inertial-Viscous regime (IV) (Eggers, 1993). When viscous effects are small compared to the inertial effects, then $Oh \tilde{} 0$ and the thinning kinetics of inviscid fluids depend on the competition between capillary pressure expelling liquid out of the neck and the inertial forces opposing it (Kovalchuk, Nowak, & Simmons, 2017). This is the so-called inertial regime (I). Pure water dripping from a nozzle of 1.75 mm, for instance, has a value for $Oh \tilde{} 0.0028$, and will, therefore, follow the inertial regime. In this regime, close enough to pinch-off, the thinning dynamics will follow the equation developed by Keller & Miksis (Keller & Miksis, 1983). This equation predicts a power-law reduction of the neck diameter in time with a 2/3 exponent (Hauner, Deblais, Beattie, Kellay, & Bonn, 2017):

$$2R_{min} = A\left(\frac{\gamma}{\rho}\right)^{\frac{1}{3}}(t_0 - t)^{\frac{2}{3}} \quad (1)$$

where $2R_{\min}$ is the diameter of the neck at its minimum thickness (Fig. 1), A is a universal prefactor, γ is the surface tension, ρ is the bulk density, t is the time and t_0 is the moment of breakup. The prefactor A shows some variability in literature (Hauner et al., 2017). Hauner et al. (2017) provided an experimentally determined value of $A = 0.9$ for pinch-off of pure liquids. A prefactor of 0.7 has also been used in literature (De Saint Vincent et al., 2012; Eggers & Villermaux, 2008). Deblais et al. (2018) have recently shown that this prefactor can vary between 0.8 and 1.2 due to nonmonotonic behavior over different orders of magnitude of time as the pinch-off is approached.

Close to the pinch-off the capillary pressure at the neck increases with decreasing R_{min} due to the larger local curvature (Kovalchuk et al., 2017). The larger capillary pressure causes a flow out of the neck region, increasing the speed at which R_{min} thins near pinch-off due to positive feedback. The flow of liquid from the neck region drags surfactants along the interface, creating a gradient in surface tension. This gradient results in a dynamic surface tension, which increases as the pinch-off point approaches and gets closer to that of pure water at small enough time scales. However, De Saint Vincent et al. (2012) found that opposed to theoretical predictions, the surface tension only increases to values close to that of pure water when the concentration of surfactants are small enough (below the critical micelle concentration (CMC)). The thinning process of slender jets sometimes causes capillary instabilities that are investigated in detail in different regimes (Eggers & Villermaux, 2008; Habibi, Rahmani, Bonn, & Ribe, 2010; Javadi, Eggers, Bonn, Habibi, & Ribe, 2013). More recently, Li and Sprittles (Li & Sprittles, 2016) provided an extensive analysis of the transition between different regimes close to the capillary breakup of a liquid jet. However, as in this study surfactant molecules are used in aqueous solutions with negligible effect on bulk viscosity, only the I regime will be discussed.

Although a large amount of research has been done on studying the pinch-off dynamics of pure liquids, with well-defined surface tension, the behavior of surfactant-laden interfaces close to pinch-off has been studied only in recent years. Most of these studies have focused on low molecular weight surfactants (Ambravaneswaran & Basaran, 1999; Craster, Matar, & Papageorgiou, 2009; Kovalchuk, Jenkinson, Miller, & Simmons, 2018; Kovalchuk, Nowak, & Simmons, 2016; Liao, Subramani, Franses, & Basaran, 2004; McGough & Basaran, 2006; Ponce--Torres, Montanero, Herrada, Vega, & Vega, 2017; Roché, Aytouna, Bonn, & Kellay, 2009; De Saint Vincent et al., 2012; Xu, Liao, & Basaran, 2007) that present viscoelasticity due to changes in surface pressure, but generally do not form interfacial structures. This means that the dilatational properties of these interfaces stabilized by LMWS are explained by the Lucassen-van den Tempel model, which accounts for the subsurface mass transfer via Fickian Diffusion (Lucassen & Van Den Tempel, 1972a; 1972b), while the shear properties of LMWS are usually relatively low (Sagis, 2011) due to weak lateral interactions (Bos & Van Vliet, 2001). In real life applications, however, there are many examples of large surfactants or surface-active bio-polymers that are able to form viscoelastic 2D structures through lateral interactions such as hydrophobic, electrostatic or covalent bonding, causing significant viscoelastic surface stresses. The available literature on fast and large deformations of viscoelastic interfaces that form 2D structures at the interface is rather scarce (Alvarado, Bidhendi, Garcia-olvera, Morin, & Oakey, 2014; Hoyer & Alvarado, 2017; Zhao, Miller, Cooper-White, & Middelberg, 2011; Zhao et al., 2012).

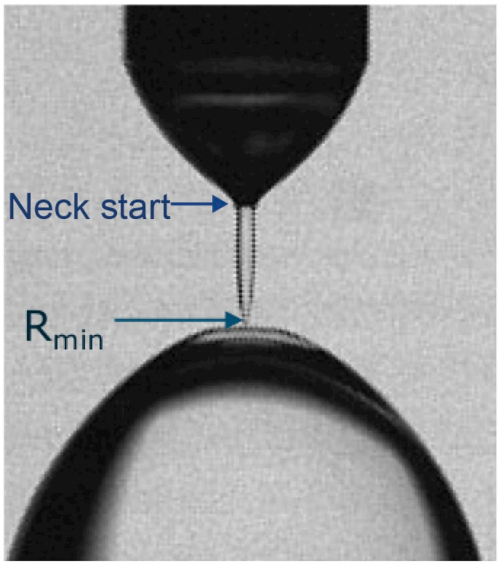

Fig. 1. Representation of where the minimum radius (R_{min}) is measured during pinch-off, and the start of the neck considered for measuring the length to R_{min}.

In this work, we study the pinch-off of liquid droplets in the presence of surface-active molecules to see how a viscoelastic interface affects the formation of droplets and the thinning dynamics of a liquid neck. Using a high-speed imaging method we look at the pinch-off of aqueous solutions of low molecular weight surfactants (SDS, Tween 20), proteins ($\beta - Lg$, BSA), and the saponin Escin. We then compare surface shear rheology measurements of Escin to the observed shape, as Escin showed the largest effect on pinch-off. Studying the effects of interfacial rheology on droplet formation at short time scales is highly relevant for food products, as a way to look into fast and large deformations of interfaces. This is of interest for food processes as the measurements outside the linear viscoelastic regime are seldom performed, but are relevant for common food processes such as chewing and swallowing (Melito & Daubert, 2012), or emulsifying and foaming. As such, the technique we use here can provide insight into the foamability and emulsifiability of formulations. But it also draws the attention to the need for more interfacial rheology studies that look into deformations outside the linear viscoelastic regime of interfaces relevant for food products.

2. Materials and methods

All materials used in this work were purchased from Sigma-Aldrich Co., Missouri, USA, including Sodium dodecyl sulfate (with $\geq$ 98.5% purity, product no. L3771), Tween 20 (Polyethylene glycol sorbitan monolaurate, viscous liquid, product no. P1379), Escin (with $\geq$ 95% purity, product no. E1378), Bovine Serum Albumin (lyophilized powder with $\geq$96% purity, product no. A4503), and β-Lactoglobulin (β-Lactoglobulins A and B chromatographically purified, lyophilized with $\geq$ 90% purity, product no. L3908). The surfactants and surface active biopolymers were used without further purification. Pure water (Milli-Q) was used as a reference and to check the accuracy of the pinch-off measurements. Solutions were prepared at 0.1 times the Critical Micelle Concentration (CMC), 0.5 CMC, 1 CMC and 2 CMC, for SDS, Tween 20 and Escin. The concentrations corresponding to 1 CMC were 8.03 mM for SDS (Chatterjee, Moulik, Sanyal, Mishra, & Puri, 2001), 0, 06 mM for Tween 20 (provided by manufacturer) and 0.07 mM for Escin (Golemanov, Tcholakova, Denkov, Pelan, & Stoyanov, 2013). For the proteins and Escin different concentrations (0.05 $g\,L^{-1}$, 0.5 $g\,L^{-1}$, and 5 $g\,L^{-1}$) in phosphate buffer 10 mM at pH 7 were also prepared. Escin at a concentration of 5 $g\,L^{-1}$ in phosphate buffer 10 mM at pH 7 was used for the surface rheology experiments. All surfactants and protein solutions were prepared fresh and used on the same day. The (bulk) viscosity and density of the solutions at concentrations mentioned were assumed to be the same as water.

The effect of the surface-active molecules on the capillary breakup of drops was studied using a high-speed camera to measure the evolution of the neck diameter over a few milliseconds before pinch-off. The experimental setup for the pinch-off experiment comprised a high-speed video camera (Phantom v710 Vision Research, Wayne, USA) with a mounted objective Canon Macro 100 *mm* (Canon, Japan). A resolution of 256· 256 pixels was used, at 70,000 frames-per-second (fps) and exposure time of 13.916 μs. A 30 *mL* syringe with a 1.75 *mm* outer diameter nozzle was used, together with a syringe pump (PHD 4400 Harvard Apparatus, Massachusetts, USA) to provide a constant creation of droplets with a rate of 0.5 $mL\,h^{-1}$. To capture a clear image of the droplet edge, an LCD backlight consisting of 4 strips with 2853 SMD LEDs (0.2W 3V) with 48 LEDs per strip was used. The LED strips were positioned at the edges of a plastic diffuser sheet with a reflective sheet at the back. For the droplets of the samples containing proteins or Escin, aging of the interface before pinch-off was also considered. Aging time (τ) of 2400 s were used, and the evaporation was compensated by very slow pumping from the reservoir into the droplet to maintain a constant size. After the aging process, a flow rate of 0.5 $mL\,h^{-1}$ was used to cause the breakup and drop formation. The recorded movies were treated as tiff images and binarized with Matlab. For the pinch-off analysis of the droplet, the diameter of the neck, $2R_{min}$, during the thinning was measured with a Matlab code adapted and modified from Kwon et al. (2015). To calculate the thickness of the neck, the boundaries between black and white pixels were used. The distance in pixels at the minimum thickness between two points of the boundaries was measured and converted to *mm* with a conversion factor obtained from ImageJ (Rueden et al., 2017).

The surface rheology measurements of air-solution interfaces stabilized by Escin were performed using an AR-G2 rotational rheometer (TA Instruments, DE, USA). A double wall ring geometry (DWRG) was used with a circular channel containing 18.8 *mL* of the sample. A Pt/Ir alloy ring with a diamond shape cross-section was then placed at the air-water interface. Amplitude sweeps were performed on aged samples (τ = 2400), at frequencies of 0.1 and 1 Hz with applied strains ranging from 0.01 to 40%. At strain domains where the shear elasticity was in the linear regime, frequency sweeps were also performed from 0.005 to 10 *Hz* to study the frequency dependence. The surface shear storage *G*' and loss *G*'' modulus were obtained using the first harmonic of the oscillating stress signal. All experiments were performed at 20 °C. The circular channel and ring were rinsed with MilliQ water and ethanol before each test. Finally, the ring was flamed to ensure removal of any organic contamination.

3. Experimental results

3.1. Capillary breakup

The dynamics of neck thinning in the inertial regime provides a method to calculate the effective dynamic surface tension of the liquid γ_{eff} at *ms* timescales. According to equation (1), close to the pinch-off, the slope of the linear fit of $(2R_{min})^{3/2}$ as a function of $(t_0 - t)$, determines γ_{eff}. In this study we use the universal prefactor $A = 0.9$, determined experimentally by (Hauner et al., 2017). The effective surface tensions and standard deviation are averaged and calculated over nine independent measurements.

3.1.1. Breakup of SDS, tween 20 and escin solutions

Two commonly used surfactants (SDS, 288.38 $g\,mol^{-1}$ and Tween 20, 1225 $g\,mol^{-1}$) with significant differences in their molecular weights and diffusion coefficients were chosen to study their effect on the capillary breakup of their solutions. The diffusion coefficients found in literature for these molecules are $7.2{\cdot}10^{-10}\ m^2\,s^{-1}$ for SDS (Staggemeier, Collier, Prazen, & Synovec, 2005) and $3.7{\cdot}10^{-10}\ m^2\,s^{-1}$ for Tween 20 (Biswal & Singh, 2016). The triterpenoid saponin Escin with a molecular weight of 1131.269 $g\,mol^{-1}$ was also chosen, which has previously shown to have very high shear and dilatational viscoelastic moduli (Golemanov et al., 2013; Pagureva et al., 2016; Tcholakova et al., 2017). Escin is a monodesmosidic (one sugar chain attached to the aglycone) triterpenoid saponin (Böttcher & Drusch, 2017). The diffusion coefficient of Escin was not found in literature, but for other saponins a range of values from $2{\cdot}10^{-10}\ m^2\,s^{-1}$ to $2.8{\cdot}10^{-10}\ m^2\,s^{-1}$ is reported (Irigoyen & Giner, 2018; Stanimirova et al., 2011). The three LMWS form micelles above a certain CMC and the concentrations were normalized by their CMC. The equilibrium surface tension of these surfactants at the different concentrations can be found in literature, and have been included in Table 1.

Images of neck thinning for pure water and surfactant solutions at 2 CMC approaching pinch-off are presented in Fig. 2. The formed droplets for surfactant solutions are smaller with respect to the pure water droplet, due to lower surface tension of the surfactant solutions. The images at 7.5 *ms* before pinch-off show a thinner neck for surfactant solutions compared to pure water (data for whole recorded thinning over 70 *ms* provided in supplementary material). This means that in the last few milliseconds before the pinch-off, the thinning kinetics or the rate of decreas of the neck diameter is slower for surfactant solutions.

Table 1
Equilibrium surface tension values found in literature for the different surfactants and concentrations used.

Concentration	SDS[a]	Tween 20[b]	Escin[c]
0.1 CMC	65 $mN\,m^{-1}$	53 $mN\,m^{-1}$	62 $mN\,m^{-1}$
0.5 CMC	41 $mN\,m^{-1}$	45 $mN\,m^{-1}$	56 $mN\,m^{-1}$
1 CMC	35 $mN\,m^{-1}$	35 $mN\,m^{-1}$	46 $mN\,m^{-1}$
2 CMC	34 $mN\,m^{-1}$	35 $mN\,m^{-1}$	44 $mN\,m^{-1}$

[a] (H. Zhao et al., 2017).
[b] (Niño & Patino, 1998).
[c] (Pagureva et al., 2016).

We know that the addition of surfactants at the concentrations used in the experiments have a negligible effect on the bulk viscosity and density of the solutions. Therefore, the bulk viscosities are comparable to that of pure water, thus, the pinch-off occurs in the inertial regime. This is also indicated by the linear shape of the curves in Fig. 3, where $(2R_{min})^{3/2}$ is plotted as a function of time to pinch-off for the three surfactant solutions. The slope of fitted lines is proportional to $A^{3/2}(\gamma_{eff}/\rho)^{1/2}$ (Hauner et al., 2017), from which γ_{eff} can be obtained. The linear thinning spans mostly over the last 1.5 *ms*, and shows a slight deviation from linearity for time intervals above $1.5-2$ *ms*. Therefore, linear fits to the last 1.5 *ms* have been used to calculate the γ_{eff} and the results are shown in Fig. 4. The horizontal blue line corresponds to $\gamma_{eff} = 88.4 \pm 0.2\ mN\,m^{-1}$, calculated from pinch-off data of pure Milli-Q water. This is close to the value obtained by Hauner et al. (2017) for pure water (γ_{eff}~$90\ mN\,m^{-1}$), using the same prefactor ($A = 0.9$). This surprising value was found in (Hauner et al., 2017) for newly formed interfaces at small timescales of water at different pH and with the addition of NaCl, and is not the equilibrium value of γ~$72\ mN\,m^{-1}$ commonly found. The authors in (Hauner et al., 2017) hypothesized that this value might be associated with adsorption effects of protons or hydroxides at the surface. Although the effective surface tension of the three solutions decrease with increasing concentrations as expected, they show different trends.

SDS shows the fastest decrease in the effective surface tension as a function of concentration. It reaches a plateau at a concentration of 1 CMC and remains roughly the same up to 2 CMC. These values are in agreement with the equilibrium surface tension (γ_{eq}) of 35 $mN\,m^{-1}$

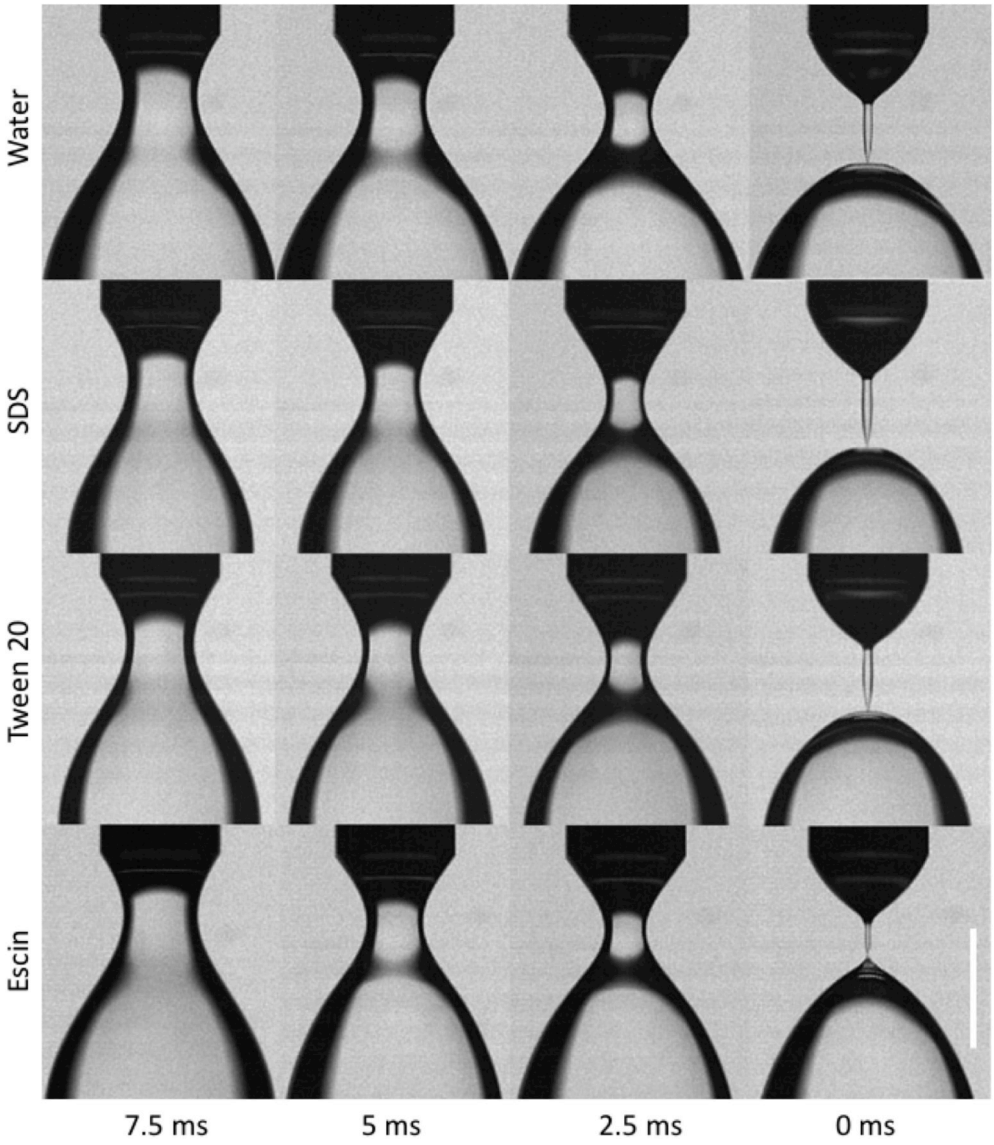

Fig. 2. Droplet thinning for pure water and different surfactants (SDS, Tween 20, Escin) at concentration of 2CMC. Time to pinch-off shown at the bottom of each column in ms. White scale bar at the bottom right corner corresponds to 1.75 *mm*.

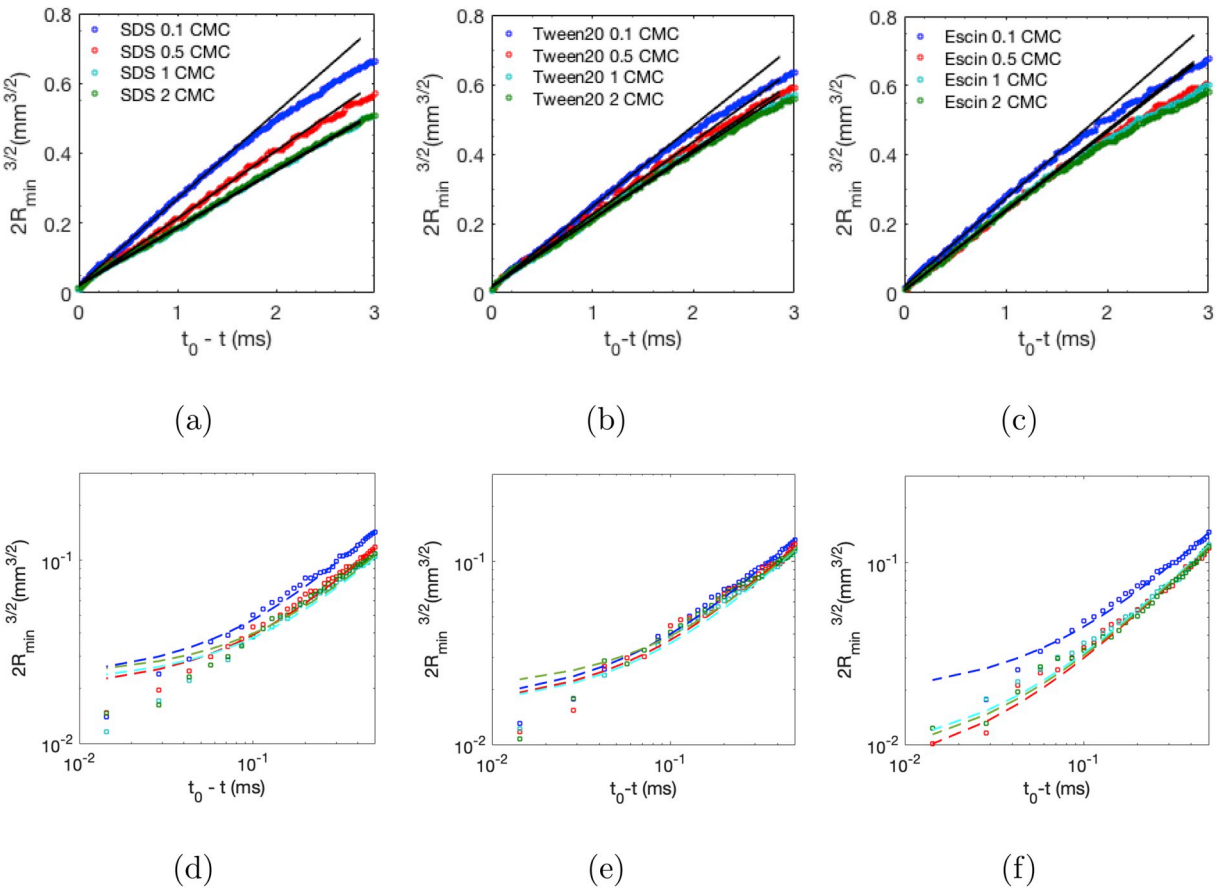

Fig. 3. Diameter of the neck to the power 3/2 as function of time to pinch-off for (a) SDS, (b) Tween 20, and (c) Escin. Thinning slopes fitted to the last 1.5 *ms* for each of the surfactants, at concentrations normalized by CMC. (d), (e) and (f) are showing the same data as (a), (b), and (c) respectively, in log-log scale and a magnification of the last 0.5 *ms*.

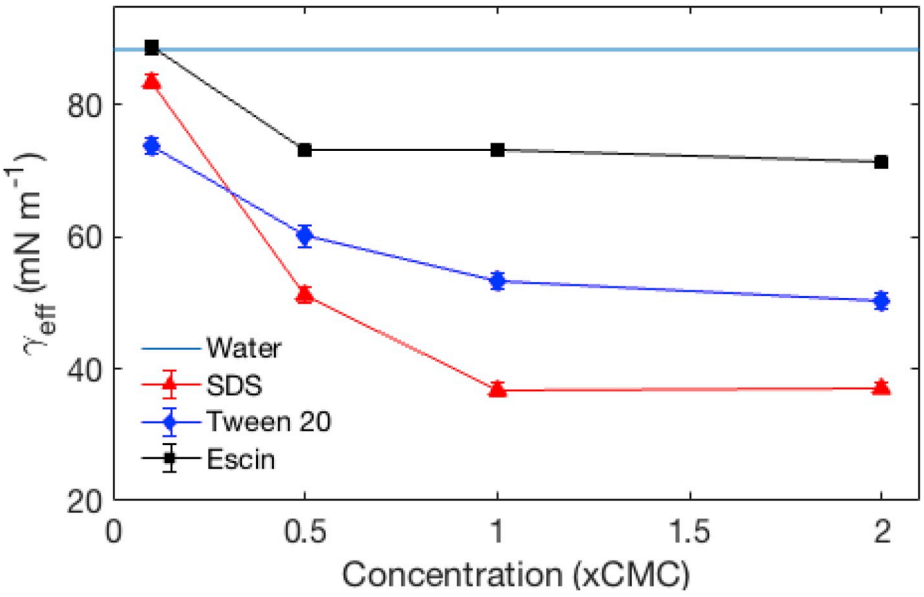

Fig. 4. Effective surface tension (γ_{eff}) as function of concentration in CMC. γ_{eff} is calculated from the thinning slope in the last 1.5 *ms* using eq. (1).

reported in literature (H. Zhao, Zhang, Xu, Li, & Liu, 2017). This indicates that SDS molecules adsorb fast enough to the interface and keep the surface tension constant until < 0.05 *ms* before pinch-off, where a small deviation from a straight line is observed. This deviation will be explained in more detail later. In other studies where the dynamic surface tension of SDS solutions (~0.5 CMC in 100 *mM* NaCl) were measured using the oscillating jet method at *ms* timescales, a surface tension of $\gamma = 49 mN\, m^{-1}$ was obtained (Fainerman & Lylyk, 1983). This

value is comparable with $\gamma_{eff} = 51\ mN\ m^{-1}$ that we obtained at 0.5 CMC. Higher surface tension values were also reported in literature for SDS in water without salts: $\gamma \sim 60 mN\ m^{-1}$ (~0.5 CMC, (Thomas & Potter, 1975)) and $\gamma \sim 70 mN\ m^{-1}$ (~0.5 CMC (Owens, 1969),). This can be due to the fact that in the oscillating jet method the surface is constantly renewed, while in droplet pinch-off the slow flow allows for some adsorption of surfactant. Therefore, Marangoni stresses are expected to play a more important role in droplet pinch-off. Furthermore, in (Fainerman & Lylyk, 1983) the authors found little difference in the dynamic surface tension when increasing the concentrations from 1.14 to 2.3 CMC, which is comparable to the plateau we observe in Fig (4) from 1 CMC to 2 CMC.

Although the equilibrium surface tension of Tween 20 is comparable with that of SDS solutions, the measured γ_{eff} for Tween 20 are 53.3 ± 1.1 and $50.3 \pm 1.2\ mN\ m^{-1}$ for 1 and 2 CMC, respectively. These values are higher compared to SDS solutions, and this can be attributed to the higher diffusion coefficient of SDS ($7.2{\cdot}10^{-1}\ m^2 s^{-1}$ (Staggemeier et al., 2005)) compared to Tween 20 ($3.7{\cdot}10^{-1}\ m^2 s^{-1}$ (Biswal & Singh, 2016)). However, at 0.1 CMC Tween 20 has a smaller γ_{eff} than SDS, which seems counter-intuitive based on the smaller diffusion coefficient and lower CMC of Tween 20. An explanation for this is that at this low concentration the diffusion is less important than the adsorption, and the air-water interface carries a negative charge due to the hydroxide ions (Ciunel, Armelin, Findenegg, & Von Klitzing, 2005), posing an adsorption barrier for the anionic SDS but not for the non-ionic Tween 20. As the concentration is increased, the diffusion plays a larger role than adsorption.

Escin has a molecular weight similar to that of Tween 20, but it shows a smaller rate of decrease in γ_{eff} as a function of concentration. This can be explained by the lower diffusion coefficient of saponins, which are in the range $2 - 2.8{\cdot}10^{-1}\ m^2 s^{-1}$ (Irigoyen & Giner, 2018; Stanimirova et al., 2011). Furthermore, slower adsorption of the triterpenoid *Quillaja* saponin compared to SDS and Tween 20 has been observed before at small timescales, attributing it to a barrier-controlled adsorption (Stanimirova et al., 2011), which agrees with the results observed here.

Although Escin shows a plateau in the measured effective surface tension at concentrations of 0.5 CMC and higher, the breakup images just before detachment for 0.5 CMC to 2 CMS are significantly different (Fig. 5). The breakup images just before detachment also reveal a remarkable difference between pinch-off of Escin and the other two surfactants at 2 CMC (Fig. 2). From the right hand column images in Fig. 2 it is clear that for Escin a pointy conical shape forms at the pinch-off point of the droplet while for the other solutions and pure water this is not observed. Having a closer look at the pinch-off data of SDS and Tween 20 in Fig. 3 reveals that at about 0.05 *ms* before pinch-off the slope of the curves increases slightly. Fig. 3d–e shows a zoomed in view of the data of Fig. 3a–b in log-log scale over the last 0.5 *ms*. The slight increase in the slope of the curves at ($\sim \leq 0.05$ *ms*) might be the result of the depletion of surfactant, and thus higher γ_{eff} (De Saint Vincent et al., 2012; Kovalchuk et al., 2016, 2017). However, this effect has also been observed for pure water by Kovalchuk et al. (2017) , and was explained by viscous or visco-inertial kinetics at small time scales. Interestingly, we do not observed this deviation in Fig. 3f for Escin solutions with concentration above 0.1 CMC.

3.1.2. Effect of aging

In this section we study the effect of aging of the interface on the breakup. For this purpose we use protein and Escin solutions in phosphate buffer. Two milk proteins, β-Lactoglobulin (β-Lg) ~18,000 $g\ mol^{-1}$ and Bovine Serum Albumin (BSA) ~66,000 $g\ mol^{-1}$, and Escin are dissolved in phosphate buffer of 10 *mM*at pH 7 and concentrations of 0.05 $g\ L^{-1}$, 0.5 $g\ L^{-1}$ and 5 $g\ L^{-1}$. First, we perform the pinch-off experiment on different solutions without aging and compare the results. Then for the highest concentration the effect of an aging time of 2400 *s* on the pinch-off is investigated. The images of pinch-off for the lowest and highest concentrations, and the aged interface are presented in Fig. 6. For the lowest concentrations, the breakup shape is comparable to that of pure water. When the concentration is increased, the position of the minimum radius of the neck is slightly moved towards the nozzle, slightly increasing the symmetry in all the three samples, and indicating that the length of the neck before pinch-off becomes smaller. This effect is more pronounced for Escin than for the two protein solutions. This difference is probably due to the fact that the proteins are not able to form a strong viscoelastic interface on the time scale used in this study. A similar phenomenon was observed by (Zhao et al., 2012), where drop deformation in a microchannel in the presence of β-Lg, lysozyme and β-Casein was studied. The drop residence time inside the microchannel did not provide enough time for formation of a strong viscoelastic interface by the proteins. In contrast, they also observed that a peptide with a smaller molecular size (AFD4, 2345 Da) was capable of rapidly forming a viscoelastic interface and influence the drop deformation after a sudden contraction.

The effective surface tension calculated from the slope of the linear region in Fig. 7 are summarized in Fig. 8. For β-Lg at low concentration of about 0.05 $g\ L^{-1}$, γ_{eff} decreases about 10 $mN\ m^{-1}$ compared to pure water. This is likely due to impurities in the protein sample, such as small peptides. β-Lg has a relatively small size (~18 kDa) consisting of 162 amino acid residues and is present in the monomeric form under acidic conditions < pH 3.5. But at pH 6–8, conformational changes of the protein causes the hydrophobic core to be exposed and form weak non-obligate homodimers (~ 36 kDa) (Bello, Fragoso-Vázquez, & Correa Basurto, 2016; Kontopidis, Holt, & Sawyer, 2004). BSA is the largest molecule used in this study (~ 66 kDa (Peters, 1995)). Due to its large size and lower diffusion coefficient ($5.99{\cdot}10^{-11}\ m^2\ s^{-1}$ (Magnusson, Håkansson, Janiak, Bergenståhl, & Nilsson, 2012)) compared to β-Lg ($8.13{\cdot}10^{-11}\ m^2\ s^{-1}$ (Magnusson et al., 2012)), we expect the smallest effect in lowering γ_{eff}, as can be seen in Fig. 8. At low concentration (0.05 $g\ L^{-1}$) it has no effect on the surface tension. On the other hand, Escin has a molecular weight much smaller than both proteins (1131.3 $g\ mol^{-1}$) and the diffusion coefficient of saponins is in the range $2 - 2.8{\cdot}10^{-10}\ m^2\ s^{-1}$ (Irigoyen & Giner, 2018; Stanimirova et al., 2011),

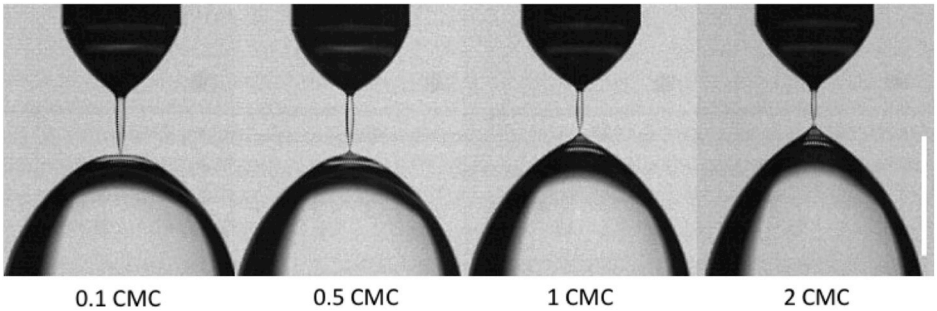

Fig. 5. Images of Escin break up at different normalized CMC concentrations just before pinch-off. White scale bar corresponds to 1.75 *mm*.

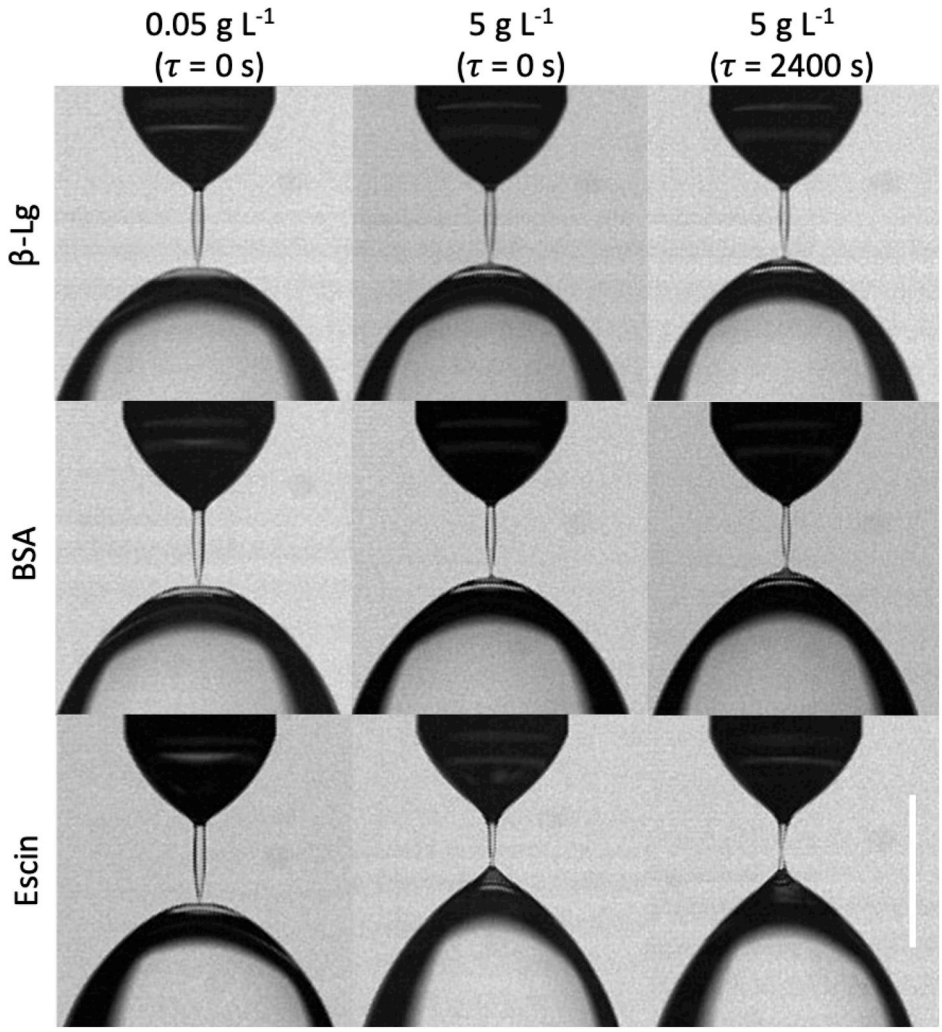

Fig. 6. Images of break up in the presence of surface active molecules (β-Lg, BSA, Escin) capable of forming a viscoelastic interface. τ represents aging time. Concentrations are shown at the top of each column. White scale bar at bottom right corner corresponds to 1.75 *mm*.

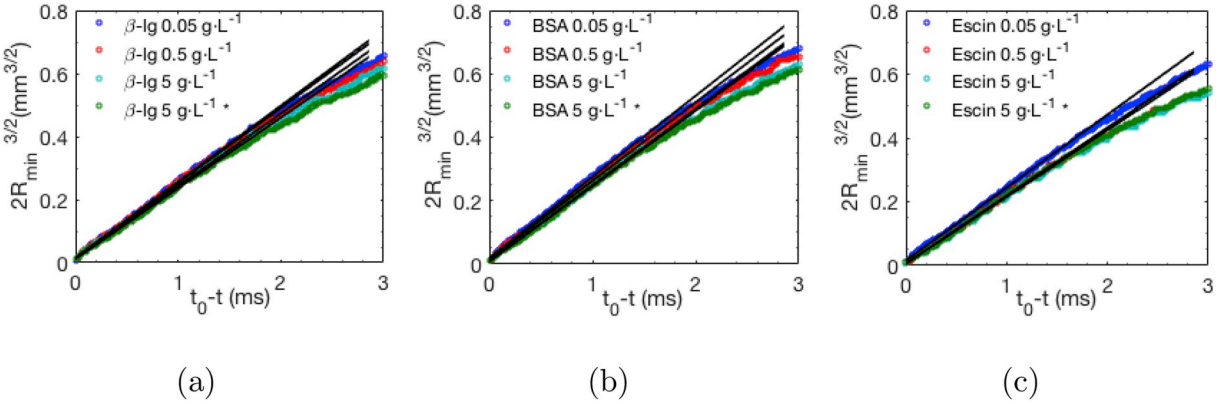

Fig. 7. Diameter of the neck to the power 3/2 as function of time to pinch-off for (a) β-Lg, (b) BSA, and (c) Escin. Thinning slopes fitted to the last 1.5*ms* for surface active molecules dissolved in phosphate buffer 10 *mM* pH 7 at different concentrations, and aging. Star (*) indicates aged interfaces (τ = 2400 s).

therefore showing the largest effect on lowering γ_{eff} at all concentrations.

For the two proteins and the Escin, the aging of the interface has a very small effect on lowering the surface tension, as measured from the pinch-off data. For Escin the effective surface tension even slightly increases after aging, within the range of the error bars. However, a change in neck shape is observed for all three samples (Fig. 6), although the effect of aging is more pronounced for Escin solutions. The aged interfaces with Escin show a conical shape, most likely due to high interfacial viscoelasticity imparted by this saponin. For this reason we looked in more detail at the thickness and length of the liquid necks (Fig. 9). Both the thickness and length decreased with increasing

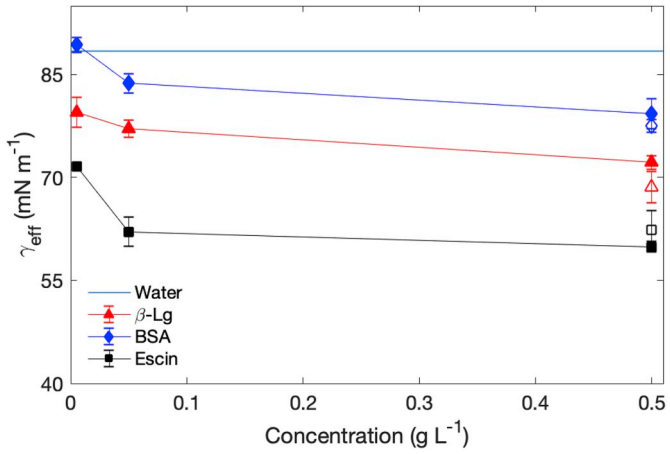

Fig. 8. Effective surface tension as calculated from the thinning slope in the last 1.5 *ms* using eq. (1). Open symbols correspond to the aged interface (τ = 2400 s).

concentration, and with aging of the interface, even for the protein samples. But the effect was more pronounced for Escin, with a neck length decreasing to more or less half (0.37 *mm*) of the length at the lower concentration (0.86 *mm*). This indicates the presence of a solid-like viscoelastic interfacial structure that remains intact in areas away from the region immediately around $2R_{min}$. The fact that we still measure effective surface tensions for the aged interfaces very similar to the non-aged ones, suggest that locally, in the area close to $2R_{min}$, this solid-like structure has yielded, and hence the dynamics is again predominantly governed by inertia, and not by the viscoelastic properties of the interface. This shows that the deformations in the pinch-off process are not just large and fast, but also significantly non-affine, and can explain why near equilibrium data for the surface properties are often such poor predictors for emulsifying ability and emulsion stability.

3.2. Surface shear rheology

Escin solutions showed the most significant effect on droplet pinch-off compared to the milk proteins upon aging. This could be attributed to the fact that interfaces stabilized by milk proteins show a much lower elasticity (both shear and dilatational) than air-water interfaces stabilized by Escin. For example, milk protein stabilized interfaces have a surface shear elastic modulus, usually between 10 and 100 mNm^{-1} (Bos & Van Vliet, 2001; Cascao Pereira, Théodoly, Blanch, & Radke, 2003; Petkov, Gurkov, Campbell, & Borwankar, 2000; Sagis, 2011), while the surface shear elastic modulus of Escin is typically above 1000 mNm^{-1}. We performed surface shear rheology measurements on Escin solution, in which the surface shear storage (G') and loss modulus (G'') were measured for aged (τ = 2400 s) samples at concentrations of 5 $g\,L^{-1}$, and the results are shown in Fig. 10a. The data at small deformation (ε) shows very high elastic and viscous moduli, which is in agreement with previous studies for Escin and other saponins solutions. For our samples we observe higher values for both G' and G'', (1097 $mN\,m^{-1}$ and 57 $mN\,m^{-1}$ respectively, at 0.02% strain and 1 *Hz*) compared to the values observed by Golemanov et al. (2013). This is expected because of the longer aging times used in our study (40 min), as opposed to the 30 min used in. Both G' and G'' are similar to those observed in (James et al., 2018). These values are indeed significantly higher than those observed for interfaces stabilized by milk proteins (Bos & Van Vliet, 2001; Cascao; Cascao Pereira et al., 2003; Petkov et al., 2000; Sagis, 2011) and reflect the high elasticity of this interfacial layer, with a loss factor $\tan(\delta) = \frac{G''}{G'} = 0.05$. Therefore, we observe a strong elastic behavior for Escin. This G' value is slightly higher than that observed for asphaltenes at the air-water interface measured by DWRG (850 $mN\,m^{-1}$) (Lin et al., 2018). At an oscillation frequency of 0.1 *Hz*, a linear response is observed up to $\approx$ 0.40% strain, and this value decreases at a frequency of 1 *Hz*, with a linear domain up to $\approx$ 0.14% strain.

Fig. 10b shows the frequency sweep at 0.02% strain on aged Escin solution. Over the whole frequency range of our measurements the interface response is predominantly elastic $G' \gg G''$. As we are interested in the fast deformations, the frequency sweeps clearly shows that Escin shows solid-like behaviour at the interface during breakup.

The high elastic and viscous responses of Escin solutions are due to the strong interactions between Escin molecules at the interface (Tsibranska, Ivanova, Tcholakova, & Denkov, 2017). At higher deformation strains, the elastic response decreases, indicating that surface structures are broken, while the dissipation in the form of a viscous response increases. A crossover from solid-like behaviour to fluid-like occurs when $G'' > G'$, at $\approx$ 1.2% deformation. At this strain, a viscous overshoot with a peak G'' value is observed for both frequencies. This increase in viscous dissipation is probably due to rearrangements of the more unstable clusters or domains under shear as was seen before in (Golemanov et al., 2013). By increasing the deformation, both G' and G'' further decrease with increasing strain as the interfacial structures are broken down.

This large decrease in G' value in the nonlinear regime (three orders of magnitude), and the associated transition to weak viscous behavior, can explain why in the results of the pinch-off experiments of Escin we still find that the dynamics are governed by inertia, and effective surface tensions are similar to those for non-aged samples, in spite of seeing

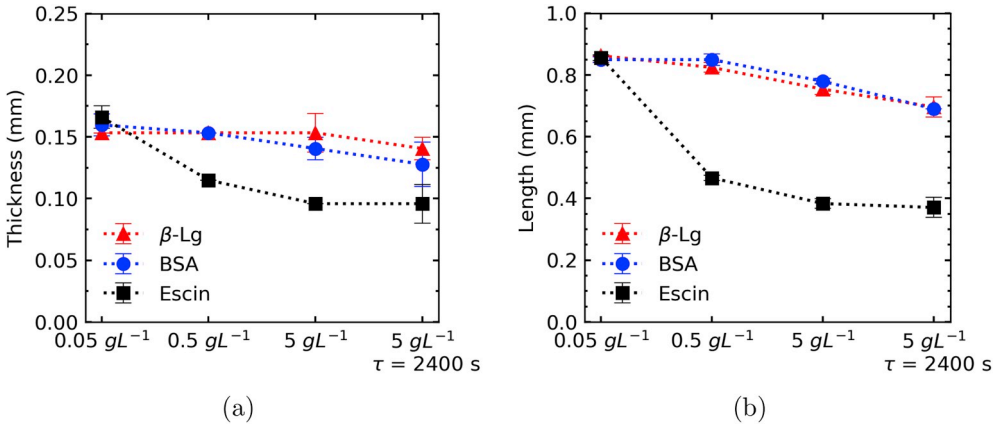

Fig. 9. (a) Thickness of the liquid neck in the middle region and (b) length of the liquid neck, from the start of the neck to R_{min}. Data obtained from the images just before pinch-off for the samples for which the aging of the interface was studied (β-Lg, BSA, and Escin). Data are averaged over three independent measurements and the standard deviation.

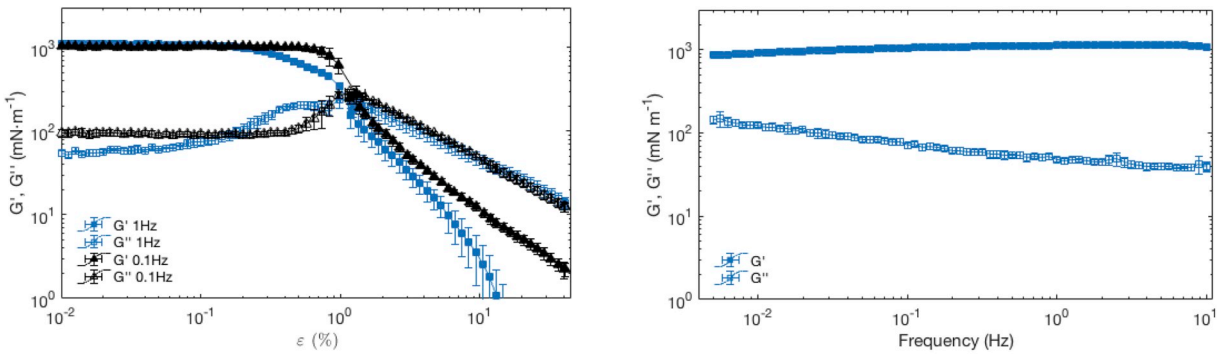

(a) (b)

Fig. 10. Amplitude sweep from 0.01% to 40% strain (a) and frequency sweep performed at 0.02% strain (b). *G*' is the shear storage (or elastic) mudulus, and *G*'' the loss (or viscous) modulus. Averages and standard deviation calculated from three measurements.

differences in the shape of the liquid necks. The conical neck is due to the high elasticity of this interface, and due to the fact that the deformation is non-affine, the moduli remain relatively high, and the structure does not yield in the region outside R_{min}. Within that region, the deformations are large enough, to break down the solid-like viscoelastic structure, and we observe inertial thinning. It is interesting to note, that even though the elastic moduli for the protein stabilized interfaces used here are usually almost two orders of magnitude lower (Cascao Pereira et al., 2003; Petkov et al., 2000) than the one we observed for Escin, the proteins still affected the shape of the neck. But just like for Escin, the thinning for both proteins follows inertial thinning, characterized by a 2/3 power law. Just like Escin, interfaces stabilized by these proteins show solid-like viscoelastic behavior at small (<10%) and slow deformations, and can display yielding at larger deformations, such as those occurring in the region close to R_{min}. Note that, whereas the shape changes induced by surface viscoelasticity for Escin are already somewhat visible without aging ($\tau = 0$), for the proteins these are significant only for the aged samples. It is known that for protein-stabilized interfaces the formation of a solid-like viscoelastic layer takes much longer than for Escin, and therefore without aging these effects are rather small.

4. Discussion: effect of interfacial viscoelasticity on the neck thinning

The process of neck thinning involves stretching and creation of new interface. The higher the elasticity of the interface the higher the resistance against stretching the interface and the lower the rate of new surface creation. The surface shear measurements confirm the high interfacial viscoelasticity of Escin at the air/water interface. This means that Escin in comparison with other surfactants with low surface elasticity shows more resistance against surface stretching and creation. As one can see from the images before pinch-off of Escin solutions (Figs. 2, 5 and 6), the creation of new interface is greatly reduced compared to SDS and Tween 20. The increase in the viscoelasticity of the interface and resulting increase in resistance against interfacial stretching, is greatly enhanced by aging, which manifests itself by the formation of a conical shape before pinch-off (Fig. 6).

It is known that the presence of soluble surfactants stabilize the liquid neck, slow down the pinch-off, and increase the length of the neck (De Saint Vincent et al., 2012; Kovalchuk et al., 2016). This stabilizing effect is due to both lowering of the surface tension and an increase in Marangoni stresses. Close to the pinch-off, the capillary pressure at the neck becomes very high, causing a convective flow which sweeps the surface-active molecules away from the neck region. This flow will partly deplete the region of surfactants, creating gradients in γ along the surface. The gradient of surface tension at the neck region stabilize the liquid neck (Zhang, Padgett, & Basaran, 1996). The thinner neck of Escin solutions at large concentrations indicates that the liquid neck is not stabilized by surface tension gradients. The neck is more likely stabilized by the formation of a strong viscoelastic interface. Mobility of surface molecules in a highly viscoelastic interface is hindered and the convective flow is not able to sweep the molecules at the interface, and therefore the establishment of a gradient of surface tension across the interface is prevented. This can also be confirmed by the high Boussinesq number of saponin molecules (Golemanov, Tcholakova, Denkov, Pelan, & Stoyanov, 2012). This resistance to sweeping the surface molecules away from the neck region of Escin, would explain why an increase in slope of the data at 0.05 *ms* observed for SDS and Tween 20 (Fig. 3d–e) is not observed for Escin at concentrations above 0.1 CMC.

The conical shape at the pinch-off point of aged Escin solution indicates that (parts of) the interface after aging behave more like a soft solid. But the fact that we do not see any changes in the dynamic surface tension as calculated from the thinning images, indicates that at R_{min} the interfacial solid structures are broken down. This results (based on the surface shear rheology data) in a significant decrease in *G*'. The equilibrium data obtained in the linear regime from interfacial rheology experiments therefore have little relevance for the actual pinch-off process, and may only affect the shape of the neck and droplet outside the immediate neighborhood of the pinch-off point. Therefore, the study of the dilatational and surface shear modulus within the linear region only, may not be a good predictor for the behavior of the interface in food related processes such as mastication, emulsification or foaming. Using faster deformation rates, as the ones used in this study, gives more insight into the dynamics of the interface. Future studies should aim at looking into fast and large deformations in order to better understand the behavior of viscoelastic interfaces in processes relevant for food science and consumption.

The conical shape we have observed here, has also been observed for thinning of a liquid bridge of aged crude oil inside a brine solution (Hoyer & Alvarado, 2017). There, this behaviour was attributed to an increase in elasticity of the liquid interface due to aging. Even though the neck thinning in our experiments always follows the inertial regime with a scaling power of 2/3 in time, the conical shape at pinch-off and the symmetric profile of the neck for Escin solutions resemble the viscous breakup regime (Royer et al., 2009). The symmetric profile was also observed by Aytouna et al. (2013), for pinch-off of yield stress fluids (emulsions) and shear-thinning fluids (using xanthan solutions). Pinch-off of shear-thickening granular suspensions, also follows a power-law exponent of 2/3 (Pan, Louvet, Hennequin, Kellay, & Bonn, 2015) with asymmetric and symmetric neck profiles for low and high volume fractions of suspensions, respectively. It seems that the symmetric shape of the neck is associated with the viscoelastic properties of

the liquid as observed for Escin; the addition of Escin results in the formation of a viscoelastic interface and increase of the neck symmetry, with an inertial thinning described by a 2/3 power. However, there is a difference between the shapes observed in our work for Escin breakup, and those of increased bulk viscosity. The main difference is in the length of the neck. When the bulk viscosity causes a symmetric neck shape, the neck would be longer (Lindner, Fiscina, & Wagner, 2015; Yildirim & Basaran, 2001) as we observe in long honey threads at the breakfast table (Eggers & Villermaux, 2008; Javadi et al., 2013). This is in contrast with the pinch-off of Escin solutions, where high surface viscoelasticity resists against stretching the interface, and results in smaller and more symmetric necks. This indicates that the thinning process here is affected by surface viscoelasticity rather than bulk viscosity. The *Oh* number of this system is still very small if only the bulk viscosity is accounted for the calculation of *Oh*.

Another important result is that the addition of Escin at concentrations higher than $0.5\ g\ L^{-1}$ completely suppressed the formation of satellite droplets. This finding might be of value for processes such as spraying, inkjet printing or microarray technology, where satellite droplets are unwanted. Affecting the satellite droplet size and decrease of the liquid neck size due to surface viscosity was also observed when an insoluble surfactant was added at the air-water interface (Ponce--Torres et al., 2017).

5. Conclusions

In this work we studied the effect of several surface active molecules (SDS, Tween 20, Escin, β-Lactoglobulin, and Bovine Serum Albumin), and aging of the interface, on the breakup dynamics with high-speed imaging of droplet pinch-off. Visualization of the process of pinch-off, reveals that the interfacial viscoelasticity of the liquid can affect the pinch-off shape and dynamics. In addition, shear interfacial rheology experiments were performed to qualitatively relate the effect of interfacial viscoelasticity to the liquid neck shape observed in the droplet formation. When the surface active molecules are not able to form 2D interfacial microstructures (e.g. SDS and Tween 20), thinning and neck formation are governed by the dynamic surface tension, as shown in previous studies.

In contrast, when 2D interfacial microstructures were formed (Escin) the interfacial viscoelasticity affects the break-up shape significantly, while the R_{min} still shows inertial thinning. We observe that interfacial viscoelasticity affects the pinch-off shape of protein solutions and Escin solution, the effect being more pronounced for the latter. The presence of elastic interfacial structures was deduced from the shape of the neck before pinch-off, and was confirmed by interfacial rheology experiments, where high G' and G'', and a low loss tangent, were observed. The high interfacial viscoelasticity completely suppressed the formation of satellite droplets by affecting the shape of the liquid neck. This is more pronounced for the aged interfaces showing higher interfacial viscoelasticity. But the fact that the measured γ_{eff} was not affected by the viscoelasticity of the interface, but the shape of the neck was, indicates that the solid interfacial structures at R_{min} are broken down. This breakdown is associted with a strong decrease in G' and G'', as seen in the strain sweeps at larger deformations. And thus the thinning at R_{min} region still follows an inertial regime, where the interfacial structures affect only the shape far from R_{min}. The equilibrium G' and G'' measured in the linear regime as most studies do, therefore show little relevance in fast and large deformation processes relevant for food sciences, such as emulsification and foaming, but also chewing or forces acting during storage or transport.

We believe that these results are important and provide new insights for processes where interfaces are undergoing very large and fast deformations, such as emulsification, foaming or 3D food printing. In addition, our results suggest opportunities to avoid undesirable satellite droplet formation, which is crucial in making mono-dispersed emulsions or improving the resolution of 3D printing.

Declaration of competing interest

None.

CRediT authorship contribution statement

Gerard Giménez-Ribes: Conceptualization, Methodology, Software, Validation, Formal analysis, Investigation, Data curation, Writing - original draft, Visualization. **Leonard M.C. Sagis:** Conceptualization, Resources, Writing - review & editing, Supervision, Project administration. **Mehdi Habibi:** Conceptualization, Resources, Writing - review & editing, Supervision, Project administration.

Appendix A. Supplementary data

Supplementary data to this article can be found online at https://doi.org/10.1016/j.foodhyd.2019.105616.

References

Alvarado, V., Bidhendi, M. M., Garcia-olvera, G., Morin, B., & Oakey, J. S. (2014). Interfacial visco-elasticity of crude oil- brine : An alternative EOR mechanism in smart waterflooding. In *SPE improved oil recovery symposium* (pp. 1–17), 1998.

Ambravaneswaran, B., & Basaran, O. A. (1999). Effects of insoluble surfactants on the nonlinear deformation and breakup of stretching liquid bridges. *Physics of Fluids, 11*(5), 997–1015.

Aytouna, M., Paredes, J., Shahidzadeh-Bonn, N., Moulinet, S., Wagner, C., Amarouchene, Y., et al. (2013). Drop formation in non-Newtonian fluids. *Physical Review Letters, 110*(3), 1–5.

Bello, M., Fragoso-Váazquez, M. J., & Correa Basurto, J. (2016). Energetic and conformational features linked to the monomeric and dimeric states of bovine BLG. *International Journal of Biological Macromolecules, 92*, 625–636.

Biswal, N. R., & Singh, J. K. (2016). Interfacial behavior of nonionic Tween 20 surfactant at oil-water interfaces in the presence of different types of nanoparticles. *RSC Advances, 6*(114), 113307–113314.

Bos, M. A., & Van Vliet, T. (2001). Interfacial rheological properties of adsorbed protein layers and surfactants: A review. *Advances in Colloid and Interface Science, 91*(3), 437–471.

Böttcher, S., & Drusch, S. (2017). Saponins — Self-assembly and behavior at aqueous interfaces. *Advances in Colloid and Interface Science, 243*, 105–113.

Cascao Pereira, L. G., Théodoly, O., Blanch, H. W., & Radke, C. J. (2003). Dilatational rheology of BSA conformers at the air/water interface. *Langmuir, 19*(6), 2349–2356.

Chatterjee, A., Moulik, S. P., Sanyal, S. K., Mishra, B. K., & Puri, P. M. (2001). Thermodynamics of micelle formation of ionic surfactants: A critical assessment for sodium dodecyl sulfate, cetyl pyridinium chloride and dioctyl sulfosuccinate (Na salt) by microcalorimetric, conductometric, and tensiometric measurements. *Journal of Physical Chemistry B, 105*(51), 12823–12831.

Christanti, Y., & Walker, L. M. (2001). Surface tension driven jet break up of strain-hardening polymer solutions. *Journal of Non-newtonian Fluid Mechanics, 100*(1–3), 9–26.

Ciunel, K., Armelin, M., Findenegg, G. H., & Von Klitzing, R. (2005). Evidence of surface charge at the air/water interface from thin-film studies on polyelectrolyte-coated substrates. *Langmuir, 21*(11), 4790–4793.

Craster, R., Matar, O., & Papageorgiou, D. (2009). Breakup of surfactant-laden jets above the critical micelle concentration. *Journal of Fluid Mechanics, 629*, 195.

De Saint Vincent, M. R., Petit, J., Aytouna, M., Delville, J. P., Bonn, D., & Kellay, H. (2012). Dynamic interfacial tension effects in the rupture of liquid necks. *Journal of Fluid Mechanics, 692*, 499–510.

Deblais, A., Herrada, M. A., Hauner, I., Velikov, K. P., Van Roon, T., Kellay, H., et al. (2018). Viscous effects on inertial drop formation. *Physical Review Letters, 121*(25), 254501.

Eggers, J. (1993). Universal pinching of 3D axisymmetric free-surface flow. *Physical Review Letters, 71*(21), 3458–3460.

Eggers, J., & Villermaux, E. (2008). Physics of liquid jets. *Reports on Progress in Physics, 71*(3), 1–79.

Fainerman, V., & Lylyk, S. (1983). Dynamic surface tension of sodium alkylsulfate solutions. *Journal of Applied Chemistry of the USSR, 56*(6), 1199–1204.

Golemanov, K., Tcholakova, S., Denkov, N., Pelan, E., & Stoyanov, S. D. (2012). Surface shear rheology of saponin adsorption layers. *Langmuir, 28*(33), 12071–12084.

Golemanov, K., Tcholakova, S., Denkov, N., Pelan, E., & Stoyanov, S. D. (2013). Remarkably high surface visco-elasticity of adsorption layers of triterpenoid saponins. *Soft Matter, 9*(24), 5738–5752.

Habibi, M., Rahmani, Y., Bonn, D., & Ribe, N. M. (2010). Buckling of liquid columns. *Physical Review Letters, 104*(7), 2–5.

Hauner, I. M., Deblais, A., Beattie, J. K., Kellay, H., & Bonn, D. (2017). The dynamic surface tension of water. *Journal of Physical Chemistry Letters, 8*(7), 1599–1603.

Hoyer, P., & Alvarado, V. (2017). Stability of liquid bridges with elastic interface. *RSC Advances, 7*, 49344–49352.
Irigoyen, R. M., & Giner, S. A. (2018). Extraction kinetics of saponins from quinoa seed (Chenopodium quinoa Willd). *International Journal of Food Studies, 7*(2), 76–88.
James, E., Tangparitkul, S., Brooker, A., Amador, C., Graydon, A., Vaccaro, M., et al. (2018). Accelerated spreading of inviscid droplets prompted by the yielding of strongly elastic interfacial films. *Colloids and Surfaces A: Physicochemical and Engineering Aspects, 554*(July), 326–333.
Javadi, A., Eggers, J., Bonn, D., Habibi, M., & Ribe, N. M. (2013). Delayed capillary breakup of falling viscous jets. *Physical Review Letters, 110*(14), 1–4.
Keller, J. B., & Miksis, M. J. (1983). Surface tension driven flows. *SIAM Journal on Applied Mathematics, 43*(2), 268–277.
Kontopidis, G., Holt, C., & Sawyer, L. (2004). Invited review: β-Lactoglobulin: Binding properties, structure, and function. *Journal of Dairy Science, 87*(4), 785–796.
Kovalchuk, N. M., Jenkinson, H., Miller, R., & Simmons, M. J. (2018). Effect of soluble surfactants on pinch-off of moderately viscous drops and satellite size. *Journal of Colloid and Interface Science, 516*, 182–191.
Kovalchuk, N. M., Nowak, E., & Simmons, M. J. (2016). Effect of soluble surfactants on the kinetics of thinning of liquid bridges during drops formation and on size of satellite droplets. *Langmuir, 32*(20), 5069–5077.
Kovalchuk, N. M., Nowak, E., & Simmons, M. J. (2017). Kinetics of liquid bridges and formation of satellite droplets: Difference between micellar and bi-layer forming solutions. *Colloids and Surfaces A: Physicochemical and Engineering Aspects, 521*, 193–203.
Kwon, K. S., Yang, L., Martin, G. D., Castrejón-Garcia, R., Castrepn-Pita, A. A., & Castrejón-Pita, J. R. (2015). Visualization and measurement. In S. D. Hoath (Ed.), *Fundamentals of inkjet printing (First Edit* (pp. 313–338). Weinheim, Germany: Wiley-VCH Verlag GmbH & Co. KGaA. Chap. 12.
Liao, Y.-C., Subramani, H. J., Franses, E. I., & Basaran, O. A. (2004). Effects of soluble surfactants on the deformation and breakup of stretching liquid bridges. *Langmuir, 20*(23), 9926–9930.
Lin, Y.-J., Barman, S., He, P., Zhang, Z., Christopher, G. F., & Biswal, S. L. (2018). Combined interfacial shear rheology and microstructure visualization of asphaltenes at air-water and oil-water interfaces. *Journal of Rheology, 62*(1), 1–10.
Lindner, A., Fiscina, J. E., & Wagner, C. (2015). Single particles accelerate final stages of capillary break-up. *Epl, 110*(6), 1–5.
Li, Y., & Sprittles, J. E. (2016). Capillary breakup of a liquid bridge: Identifying regimes and transitions. *Journal of Fluid Mechanics, 797*, 29–59.
Lucassen, J., & Van Den Tempel, M. (1972a). Dynamic measurements of dilational properties of a liquid interface. *Chemical Engineering Science, 27*(6), 1283–1291.
Lucassen, J., & Van Den Tempel, M. (1972b). Longitudinal waves on visco-elastic surfaces. *Journal of Colloid and Interface Science, 41*(3), 491–498.
Magnusson, E., Håkansson, A., Janiak, J., Bergenståhl, B., & Nilsson, L. (2012). Hydrodynamic radius determination with asymmetrical flow field-flow fractionation using decaying cross-flows. Part II. Experimental evaluation. *Journal of Chromatography A, 1253*, 127–133.
Mathues, W., Mcllroy, C., Harlen, O. G., & Clasen, C. (2015). Capillary breakup of suspensions near pinch-off. *Physics of Fluids, 27*(9).
McClements, D. J. (2007). Critical review of techniques and methodologies for characterization of emulsion stability. *Critical Reviews in Food Science and Nutrition, 47*(7), 611–649.
McGough, P. T., & Basaran, O. A. (2006). Repeated formation of fluid threads in breakup of a surfactant-covered jet. *Physical Review Letters, 96*(5), 1–4.
Melito, H., & Daubert, C. (2012). Rheological innovations for characterizing food material properties. *Annual Review of Food Science and Technology, 2*(1), 153–179.
Niño, M. R. R., & Patino, J. M. R. (1998). Surface tension of bovine serum albumin and tween 20 at the air-aqueous interface. *Journal of the American Oil Chemists Society, 75*(10), 1241.
Owens, D. K. (1969). The dynamic surface tension of sodium dodecyl sulfate solutions. *Journal of Colloid and Interface Science, 29*(3), 496–501.
Pagureva, N., Tcholakova, S., Golemanov, K., Denkov, N., Pelan, E., & Stoyanov, S. D. (2016). Surface properties of adsorption layers formed from triterpenoid and steroid saponins. *Colloids and Surfaces A: Physicochemical and Engineering Aspects, 491*, 18–28.
Pahlavan, A. A., Stone, H. A., McKinley, G. H., & Juanes, R. (2019). Restoring universality to the pinch-off of a bubble. In *Proceedings of the national academy of sciences*, 201819744.
Pan, Z., Louvet, N., Hennequin, Y., Kellay, H., & Bonn, D. (2015). Drop formation in shear-thickening granular suspensions. *Physical Review E - Statistical, Nonlinear and Soft Matter Physics, 92*(5), 1–6.
Papageorgiou, D. T. (1995). On the breakup of viscous liquid threads. *Physics of Fluids, 7*(7), 1529–1544.
Peters, T. (1995). *All about Albumin: Biochemistry, genetics, and medical applications*. San Diego, CA: Academic Press.
Petkov, J. T., Gurkov, T. D., Campbell, B. E., & Borwankar, R. P. (2000). Dilatational and shear elasticity of gel-like protein layers on air/water interface. *Langmuir, 16*(8), 3703–3711.
Ponce-Torres, A., Montanero, J. M., Herrada, M. A., Vega, E. J., & Vega, J. M. (2017). Influence of the surface viscosity on the breakup of a surfactant-laden drop. *Physical Review Letters, 118*(2), 1–5.
Ravera, F., Loglio, G., & Kovalchuk, V. I. (2010). Interfacial dilational rheology by oscillating bubble/drop methods. *Current Opinion in Colloid & Interface Science, 15*(4), 217–228.
Reynaert, S., Brooks, C. F., Moldenaers, P., Vermant, J., & Fuller, G. G. (2008). Analysis of the magnetic rod interfacial stress rheometer. *Journal of Rheology, 52*(1), 261–285.
Roché, M., Aytouna, M., Bonn, D., & Kellay, H. (2009). Effect of surface tension variations on the pinch-Off behavior of small fluid drops in the presence of surfactants. *Physical Review Letters, 103*(26), 1–4.
Royer, J. R., Evans, D. J., Oyarte, L., Guo, Q., Kapit, E., Mobius, M. E., et al. (2009). High-speed tracking of rupture and clustering in freely falling granular streams. *Nature, 459*(7250), 1110–1113.
Rueden, C. T., Schindelin, J., Hiner, M. C., DeZonia, B. E., Walter, A. E., Arena, E. T., et al. (2017). ImageJ2: ImageJ for the next generation of scientific image data. *BMC Bioinformatics, 18*(1), 529.
Sagis, L. M. (2011). Dynamic properties of interfaces in soft matter: Experiments and theory. *Reviews of Modern Physics, 83*(4), 1367–1403.
Sagis, L. M., & Fischer, P. (2014). Nonlinear rheology of complex fluid-fluid interfaces. *Current Opinion in Colloid & Interface Science, 19*(6), 520–529.
Staggemeier, B. A., Collier, T. O., Prazen, B. J., & Synovec, R. E. (2005). Effect of solution viscosity on dynamic surface tension detection. *Analytica Chimica Acta, 534*(1), 79–87.
Stanimirova, R., Marinova, K., Tcholakova, S., Denkov, N. D., Stoyanov, S., & Pelan, E. (2011). Surface rheology of saponin adsorption layers. *Langmuir, 27*(20), 12486–12498.
Tcholakova, S., Mustan, F., Pagureva, N., Golemanov, K., Denkov, N. D., Pelan, E. G., et al. (2017). Role of surface properties for the kinetics of bubble Ostwald ripening in saponin-stabilized foams. *Colloids and Surfaces A: Physicochemical and Engineering Aspects, 534*(November 2016), 16–25.
Thomas, W., & Potter, L. (1975). Solution/air interfaces I. An oscillating jet relative method for determining dynamic surface tensions. *Journal of Colloid and Interface Science, 50*(3), 397–412.
Tsibranska, S., Ivanova, A., Tcholakova, S., & Denkov, N. (2017). Self-Assembly of Escin molecules at the air-water interface as studied by molecular dynamics. *Langmuir, 33*(33), 8330–8341.
Vandebril, S., Franck, A., Fuller, G. G., Moldenaers, P., & Vermant, J. (2010). A double wall-ring geometry for interfacial shear rheometry. *Rheologica Acta, 49*(2), 131–144.
Xu, Q., Liao, Y. C., & Basaran, O. A. (2007). Can surfactant be present at pinch-off of a liquid filament? *Physical Review Letters, 98*(5).
Yarin, A. (2006). Drop impact dynamics: Splashing, spreading, receding, bouncing. Is …. *Annual Review of Fluid Mechanics, 38*(1), 159–192.
Yildirim, O. E., & Basaran, O. A. (2001). Deformation and breakup of stretching bridges of Newtonian and shear-thinning liquids: Comparison of one- and two-dimensional models. *Chemical Engineering Science, 56*(1), 211–233.
Zhang, X., Padgett, R. S., & Basaran, O. A. (1996). Nonlinear deformation and breakup of stretching liquid bridges. *Journal of Fluid Mechanics, 329*(-1), 207.
Zhao, C.-X., Miller, E., Cooper-White, J. J., & Middelberg, A. P. J. (2011). Effects of fluid-fluid interfacial elasticity on droplet formation in microfluidic devices. *AIChE Journal, 57*(7), 1669–1677.
Zhao, C.-X., Rondeau, E., Cooper-White, J. J., & Middelberg, A. P. J. (2012). Microfluidic elucidation of the effects of interfacial rheology on droplet deformation. *Industrial & Engineering Chemistry Research, 51*(4), 2021–2029.
Zhao, H., Zhang, W. B., Xu, J. L., Li, W. F., & Liu, H. F. (2017). Surfactant-laden drop jellyfish-breakup mode induced by the Marangoni effect. *Experiments in Fluids, 58*(3), 1–7.